Linewidth of electromagnetically induced transparency under motional averaging in a coated vapor cell*

Xu Zhi-Xiang(徐智翔)[a)], Qu Wei-Zhi(曲伟智)[a)], Gao Ran(高 然)[b)], Hu Xin-Hua(胡新华)[b)], and Xiao Yan-Hong(肖艳红)[a)†]

[a)] *Department of Physics, State Key Laboratory of Surface Physics, Laboratory of Advanced Materials, and Key Laboratory of Micro and Nano Photonic Structures of Ministry of Education, Fudan University, Shanghai* 200433, *China*
[b)] *Department of Material Science, Fudan University, Shanghai* 200433, *China*

(Received 12 October 2012; revised manuscript received 30 November 2012)

The linewidth of electromagnetically induced transparency (EIT) in a coated Rb vapor cell was studied under a magnetic field gradient. The nonlinear broadening of the EIT linewidth with the magnetic field gradient was observed. It was found that the motional averaging of the field gradient was more pronounced at higher laser intensities and larger beam sizes. In the same regime, there was a small linewidth decrease with the increasing magnetic field gradient. We have established a Monte–Carlo model, which gave results in good qualitative agreement with our experiment. Physics pictures for the above phenomena were also suggested. These results provide an understanding of the EIT linewidth behavior under motional averaging, and should be useful for applications in quantum optics and metrology based on coated vapor cells.

Keywords: electromagnetically induced transparency, coated cell, linewidth, motional averaging

PACS: 32.70.Jz, 32.80.Qk, 42.50.Gy, 42.62.Fi **DOI:** 10.1088/1674-1056/22/3/033202

1. Introduction

Manipulation of the quantum states of atomic spins and light through coherent atom–light interactions is at the heart of modern atomic and optical physics research. The electromagnetically induced transparency (EIT)[1] is one of the most frequently used processes. Such controlled interactions have applications in both quantum information science and precision measurements such as atomic frequency standards and magnetometry. Atomic vapor cells provide an interesting platform for this research due to their relative simplicity in system construction and relatively long coherence lifetime. Although the thermal motion reduces the coherence lifetime, buffer gas or anti-relaxation wall coating can greatly mitigate the decoherence. A spin lifetime as long as a minute has been demonstrated in a coated cell.[2,3] The most intriguing characteristic in a coated cell is that the atoms undergo fast ballistic motion while maintaining the coherence for a long time. This has led to a number of interesting observations such as the dual-structured EIT spectrum,[4] the counter-intuitive scaling of the EIT linewidth with the laser beam size,[5] and a slow light beam splitter.[6]

The focus of this paper is to study the EIT linewidth under motional averaging, especially in the presence of a spatially inhomogeneous magnetic field. Usually, a magnetic field gradient would lead to a linewidth broadening, which happens in the interrogation volume (such as the laser beam volume) of the cell, e.g., in the case of a vacuum vapor cell without coating. In a coated cell, however, the atoms travel rapidly within the entire cell volume, which is usually much larger than the interrogation volume, and they also experience coherent phase evolution outside the laser volume. This means that the linewidth broadening can come from both inside and outside of the laser beam, and the motional averaging becomes important. Watanabe and Robinson carried out a study[7] on the motional narrowing of the Zeeman resonance both theoretically and experimentally. There, the Zeeman coherence was established by a microwave which covered the entire cell volume. In an all-optical configuration, the effects of a magnetic field gradient on the EIT and the nonlinear magneto-optical resonance have been studied[8,9] in a buffer gas cell and in a coated cell, respectively. However, a natural yet unexplored question is how the laser beam size and the laser power affect the degree of motional averaging in a coated cell. In the present work, we theoretically and experimentally investigate this problem and find the nonlinear dependence of the EIT linewidth on the magnetic field gradient. We also identify a novel phenomenon: in certain parameter regimes, the EIT linewidth even decreases with increasing magnetic field gradient. A good qualitative agreement between the theoretical and experimental results is obtained, and physics explanations are also proposed.

The typical EIT spectra in a coated cell exhibit a dual-structured lineshape, with a sharp peak on the top of a broad pedestal, as shown in both Figs. 1(b) and 4. This can be understood using an intuitive model[10,11] based on the Ramsey

*Project supported by the National Natural Science Foundation of China (Grant Nos. 61078013 and J1103204), the Shanghai Pujiang Program, China (Grant No. 10PJ1401400), the National Basic Research Program of China (Grant Nos. 2011CB921604 and 2012CB921604), and the Fudan University, China.

†Corresponding author. E-mail: yxiao@fudan.edu.cn

© 2013 Chinese Physical Society and IOP Publishing Ltd

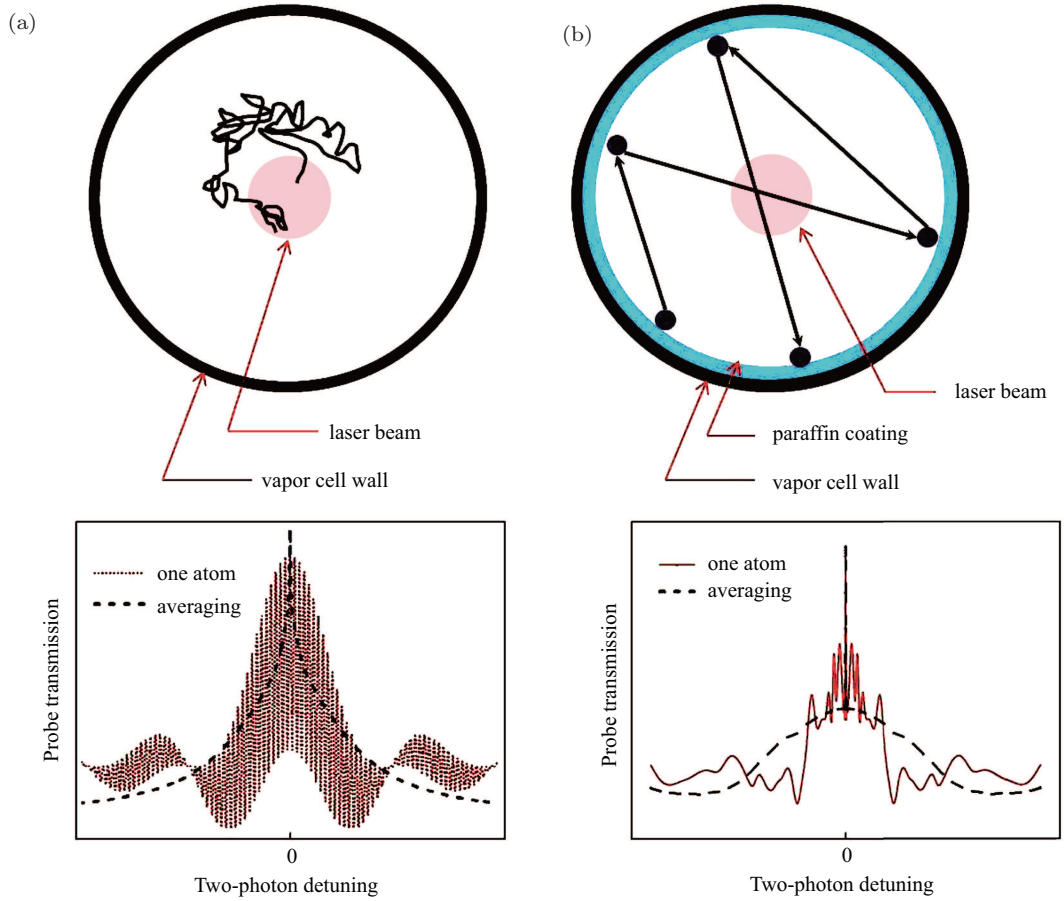


Fig. 1. (color online) Illustrations of the origin of the EIT lineshape dual structure (a) in a buffer gas cell and (b) in an anti-relaxation coated cell. The EIT spectrum from one atom shows Ramsey fringes, since it moves in and out of the laser beam, effectively seeing a Ramsey pulse sequence. Averaging over all atoms gives rise to a sharp peak above a broad pedestal. The EIT in a coated cell has a more pronounced sharp peak due to more time out of the laser beam.

spectroscopy,[12] as illustrated in Fig. 1. In a coated cell, each atom undergoes ballistic motion in and out of the laser beam, and hence also undergoes multiple interactions with the laser, with a dark time outside the laser beam between successive interactions, which gives rise to Ramsey-fringe-like EIT spectra. Averaging contributions from all atoms make the central peak stand out on the top of a pedestal, and the averaging also smears out all the fringes due to the random distribution of atomic trajectories. The linewidth of the narrow structure is mainly determined by the time that atoms spend outside the laser beam, and is eventually limited by the coherence lifetime determined by the coating quality, the cell geometry, and the dephasing processes. The broad structure linewidth is approximately the transit width associated with the single pass of the atom across the laser beam.

2. Experimental setup

Our experiment setup is similar to that in Ref. [4] and shown in Fig. 2. We used a cylindrical paraffin coated cell with enriched ^{87}Rb, 7.5 cm long and 2.5 cm wide in diameter, with a nominal T_1 time of about 0.9 s. The cell was contained in a blown air oven, which resided in a solenoid used to produce both a homogeneous magnetic field for two-photon detuning adjustments and a magnetic field gradient. The whole system was then put inside a four-layer magnetic shield which screened out stray magnetic fields with residual fields less than 2 nT. The magnetic field gradient was generated by a saddle coil similar to that used in Ref. [8]. It produced a longitudinal magnetic field gradient in the transverse direction, $\partial B_z/\partial x$. An external cavity diode laser operating at the Rb D1 line was on resonance between the ground state $5^2S_{1/2}$, $F = 2$ and the excited state $5^2P_{1/2}$, $F' = 1$. A strong control field and a weak probe field (intensity ratio of 20:1) of the same frequency but opposite circular polarization were derived from the same laser to form EIT, and the EIT spectrum was measured from the probe's transmission. For most of the data, we measured the narrow structure of the EIT to investigate the motional averaging. To avoid condensation on the wall coating of the cell body, we maintained a temperature difference between the cell body and the tail by leaving the tail outside the oven. In the experiment, we had the cell body at about 50 °C and the tail at around 41.8 °C. The temperature fluctuation was actively kept within 0.1 °C by a feedback loop.

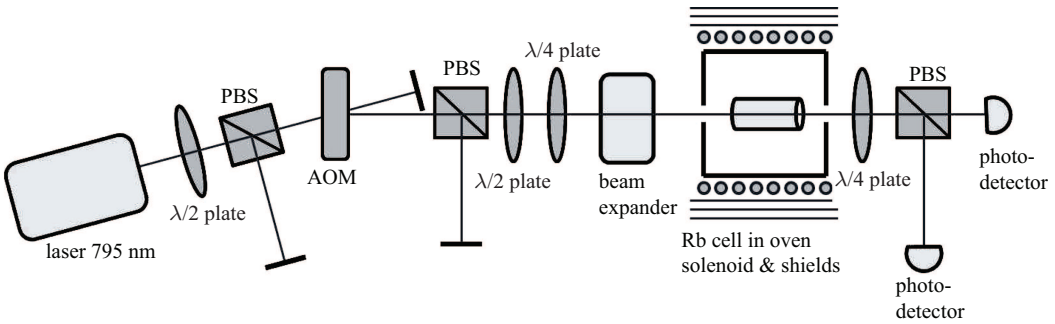


Fig. 2. Schematic diagram of the experimental setup, where PBS stands for a polarization beam splitter, and AOM stands for an acoustic-optical modulator. The homogeneous magnetic field is along the light propagation direction (defined as the z axis). The AOM is used to adjust the laser power into the cell.

3. Theoretical model

Our theoretical model is adapted from the repetitive interaction model developed by Xiao *et al.* to explain the diffusion induced Ramsey narrowing[10,11] in a buffer gas environment. This model was generalized to the coated cell case by Hohensee,[5] who used a distribution function for time in and out of the laser beam, which is suitable for a spatially homogeneous magnetic field environment. However, to take into account a spatially varying magnetic field, such as the one with a linear field gradient, the Monte–Carlo simulation of the random atomic trajectory seems to be the most applicable way.

The master equation describing the atom–light interaction in a three-level Λ system with decay processes was derived in Refs. [5], [11], and [13]. Here we only lay out the key steps. The Hamiltonian with the electric-dipole and the rotating-wave approximations is given by

$$\mathscr{H} = \hbar \begin{pmatrix} \omega_a & 0 & \Omega_{\rm p}^* \, {\rm e}^{{\rm i}\omega_{\rm p} t} \\ 0 & \omega_b & \Omega_{\rm d}^* \, {\rm e}^{{\rm i}\omega_{\rm d} t} \\ \Omega_{\rm p} \, {\rm e}^{-{\rm i}\omega_{\rm p} t} & \Omega_{\rm d} \, {\rm e}^{-{\rm i}\omega_{\rm d} t} & \omega_e \end{pmatrix}, \tag{1}$$

where ω_a, ω_b, ω_e are the frequencies (energy/$\hbar$) of three energy levels, with $|e\rangle$ being the excited state, $|b\rangle$ and $|a\rangle$ being the ground states coupled to the control (drive) and the probe fields, respectively, $\Omega_{\rm p}$ and $\Omega_{\rm d}$ are the Rabi frequencies of the probe and the control fields, and $\omega_{\rm p}$ and $\omega_{\rm d}$ are the frequencies of the probe and the control fields, respectively. After the rotating frame transformation, resetting the zero energy reference, changing the ground state basis to the dark and bright states, and adding the damping rates,[13] we have the Hamiltonian rewritten as

$$\mathscr{H} = \hbar/2 \begin{pmatrix} C_2\Delta - {\rm i}\Gamma_0 & S_2\Delta & 0 \\ S_2\Delta & -C_2\Delta - {\rm i}\Gamma_0 & -\Omega \\ 0 & -\Omega & -2\delta - {\rm i}\gamma \end{pmatrix}, \tag{2}$$

where $\Omega = \sqrt{\Omega_{\rm d}^2 + \Omega_{\rm p}^2}$, $\cos\theta = \Omega_{\rm d}/\Omega = \Omega_{\rm d}/\sqrt{\Omega_{\rm d}^2 + \Omega_{\rm p}^2}$, $\sin\theta = \Omega_{\rm p}/\Omega = \Omega_{\rm p}/\sqrt{\Omega_{\rm d}^2 + \Omega_{\rm p}^2}$, $S_2 = \sin(2\theta)$, and $C_2 = \cos(2\theta)$. Here, the one-photon detunings are $\delta_2 = \omega_{\rm d} - (\omega_e - \omega_b)$ and $\delta_1 = \omega_{\rm p} - (\omega_e - \omega_a)$, the two-photon detuning is $\Delta = \delta_1 - \delta_2$, the average one-photon detuning is $\delta = (\delta_1 + \delta_2)/2$, and Γ_0 is the intrinsic relaxation rate of the atomic ground state coherence. Then we can obtain the equation of motion of the density matrix under the Hamiltonian and a source and relaxation matrix

$$\dot{\rho} = ({\rm i}/\hbar)(\rho H^\dagger - H\rho) + (\rho_{ee}\gamma/2 + \Gamma_0/2) \begin{pmatrix} 1 & 0 & 0 \\ 0 & 1 & 0 \\ 0 & 0 & 0 \end{pmatrix}. \tag{3}$$

When $\Omega_{\rm d}$ is much smaller than the excited state decay rate γ, we can adiabatically eliminate the excited state, and reduce the system to an effective two-state system, with the two basis states being the dark state $|-\rangle$ and $|+\rangle$ which is a linear superposition of the bright and the excited states.[13] For this two-state problem, we can use the Bloch vector

$$\boldsymbol{R} = \begin{pmatrix} R_1 \\ R_2 \\ R_3 \end{pmatrix}, \tag{4}$$

which represents the population and coherence of quantum states of the two states, and is defined as

$$(R_1 + {\rm i}R_2)/2 = \rho_{-+}, \;\; R_3 = (\rho_{--}) - (\rho_{++}). \tag{5}$$

The equation of motion for the Bloch vector is

$$\mathrm{d}\boldsymbol{R}/\mathrm{d}t = \boldsymbol{T} \cdot \boldsymbol{R} + \boldsymbol{\Lambda}. \tag{6}$$

For simplicity, we consider the dephasing due to each wall collision as an infinitesimal decay, and treat the gradient magnetic field as an added term in the two-photon detuning. In this way, we can remove Γ_0 from the coefficient matrix $\boldsymbol{T}$

$$\boldsymbol{T} = \begin{pmatrix} -\alpha & -\beta' & 0 \\ \beta' & -\alpha & S_2\Delta \\ 0 & -S_2\Delta & -\alpha \end{pmatrix}, \;\; \boldsymbol{\Lambda} = \begin{pmatrix} 0 \\ 0 \\ \alpha \end{pmatrix}, \tag{7}$$

where $\beta' = -C_2\Delta$ and $\alpha = \Omega^2/(2\gamma)$ for $\delta = 0$. When the Rb atom is outside the laser beam, $\Omega = 0$, and hence $\alpha = 0$. Here, the laser beam profile is treated as a flat one with a sharp edge. The coefficient matrix $\boldsymbol{T}$ represents the physical environment interacting with the atoms, which changes with the magnetic field, the laser intensity, and the beam size.

Multiplying $\boldsymbol{U}$ from the left to both sides of Eq. (6), we have $\mathrm{d}(\boldsymbol{UR})/\mathrm{d}t = \boldsymbol{UTU}^{\dagger}\cdot\boldsymbol{UR}+\boldsymbol{U\Lambda}$, where the coefficient matrix $\boldsymbol{T}$ can be diagonalized. We define $\boldsymbol{P} = \boldsymbol{UR}$ with

$$\boldsymbol{U} = \begin{pmatrix} S_2 & 0 & C_2 \\ -\frac{1}{2}C_2 & -\frac{1}{2}\mathrm{i} & \frac{1}{2}S_2 \\ -\frac{1}{2}C_2 & \frac{1}{2}\mathrm{i} & \frac{1}{2}S_2 \end{pmatrix}. \tag{8}$$

The probe absorption coefficient is proportional to $\mathrm{Im}(\rho_{\widetilde{ea}})/\Omega_{\mathrm{p}}$, where

$$\rho_{\widetilde{ea}} = \mathrm{i}[\Omega_{\mathrm{p}}(1-R_3)+\Omega_{\mathrm{d}}(R_1-\mathrm{i}R_2)]/2(\gamma-2\mathrm{i}\delta), \tag{9}$$

and for zero averaging one-photon detuning, the probe absorption is proportional to q, with

$$q = 1-R_3+R_1\times\cos\theta/\sin\theta. \tag{10}$$

The three components of eigenvector $\boldsymbol{P}$ follow independent differential equations in the form of $\mathrm{d}\boldsymbol{P}/\mathrm{d}t = (a+bt)\boldsymbol{P}+c$,

$$\begin{cases} \mathrm{d}P_1/\mathrm{d}t = -\alpha P_1+\alpha C_2, \\ \mathrm{d}P_2/\mathrm{d}t = (\mathrm{i}\Delta-\alpha)P_2+(1/2)\alpha S_2, \\ \mathrm{d}P_3/\mathrm{d}t = (-\mathrm{i}\Delta-\alpha)P_3+(1/2)\alpha S_2, \end{cases} \tag{11}$$

where a, b, c are constants, and $\Delta = \Delta_0+kx_1+kv_xt$, with Δ_0 being the two-photon detuning excluding the magnetic field gradient, x_1 the x coordinate of the atom when $t = t_1$, and k the characteristic value of the field gradient. We have $k = g\mu_{\mathrm{B}}(\mathrm{d}B/\mathrm{d}x)/h$, where μ_{B} is the Bohr magneton, and g is the Landé g_{F} factor.

Since $\boldsymbol{P}(t)$ is a function of t, when $\boldsymbol{P}(t_1)$ is known, $\boldsymbol{P}(t_2)$ can be obtained by

$$\boldsymbol{P}(t_2) = \left[c\int_{t_1}^{t_2}F(t)\mathrm{d}t+\boldsymbol{P}(t_1)F(t_1)\right]/F(t_2), \tag{12}$$

where $F(t) = \mathrm{e}^{-at-bt^2/2}$. When the atom is outside the light beam, $\alpha = 0$, $c = 0$, and we do not need to calculate the term $\int_{t_1}^{t_2}F(t)\mathrm{d}t$. When the gradient magnetic field does not exist, $k = 0$, $b = 0$, so $F(t) = \mathrm{e}^{-at}$, and $\int_{t_1}^{t_2}F(t)\mathrm{d}t = -(\mathrm{e}^{-at_2}-\mathrm{e}^{-at_1})/a$. When the atom is inside the light beam and the gradient magnetic field exists, $b\neq 0, c\neq 0$, and we need to calculate $\int_{t_1}^{t_2}F(t)\mathrm{d}t$ numerically. Using Simpson's rule for integration, we calculate $\boldsymbol{P}(t_2)$ for a given $\boldsymbol{P}(t_1)$, and then obtain the final value of $\boldsymbol{P}$ through iteration.

In an infinitely long coated vapor cell, the Knudsen's cosine law can be used to describe the reflecting angle of an atom bouncing off the wall.[14–16] As shown in Fig. 3, the probability for the reflection angle to be ε is proportional to $\sin\varepsilon$. The time evolution of the physical quantity of one atom along its trajectory can be calculated as follows. Between two successive wall collisions, the atom moves from position (x_1,y_1) to (x_2,y_2) with a constant speed v, and the polar coordinate ϕ changes to $\phi+2\varepsilon$. At any point between the two collisions, the x coordinate satisfies $x = x_1+v_xt$. During the atomic motion, the vector $\boldsymbol{P}$ evolves according to Eq. (11). Upon collision with the wall at (x_2,y_2), the vector $\boldsymbol{P}$ is multiplied by a loss factor $\mathrm{e}^{-1/N}$. The atom is allowed to undergo N collisions with the wall, effectively experiencing a multi-pulse Ramsey sequence. Here N is randomly chosen from 4800 to 5200, which corresponds to the nominal spin lifetime of about 1 s in our cell. Then, we average over the contributions from the whole atom ensemble, and deduce the final physical quantity which gives the EIT spectrum. Finally, the narrow part of the EIT spectrum is fitted by a Lorentzian curve. In all the simulated data, the fitting uncertainty is found to be less than 1.5%.

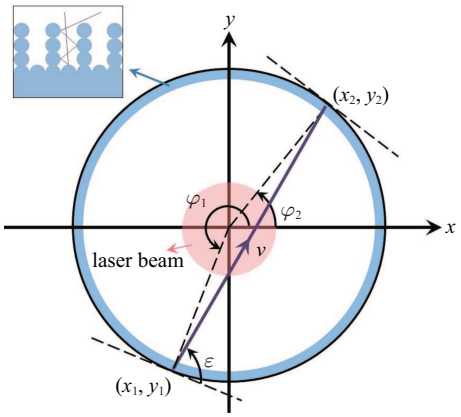


Fig. 3. (color online) Construction of the model for an infinitely long coated vapor cell. The inner circle represents the laser beam, ϕ_1 is the polar angle for position (x_1,y_1), and ϕ_2 is the polar angle for position (x_2,y_2). The ϕ changes to $\phi = \phi+2\varepsilon$ after the atom bounces off the wall, ε is the reflecting angle satisfying the Knudsen's cosine Law.

As can be seen from Fig. 3, if $\cos(\phi+2\varepsilon) > \cos(\phi)$, the velocity of the atom along the x axis is $v_x = |v\sin(\phi+\varepsilon)|$, otherwise $v_x = -|v\sin(\phi+\varepsilon)|$, where v is the average speed, $v = \sqrt{8RT/(\pi M)} = 460$ m/s, which is calculated using the Maxwell–Boltzmann distribution at the cell temperature. We deduce the displacement along the x axis between two collisions as $l = R(\cos(\phi+2\varepsilon)-\cos(\phi))$, where R is the radius of the coated vapor cell, and then we can calculate the time interval between two collisions through $t = l/v_x$.

The stochastic quantity is the key for a Monte–Carlo simulation. In our model, we generate a series of stochastic quantities distributed from 0 to 1 to obtain the stochastic bouncing angle, the number of collisions, the polar angles for the initial positions of the atom on the wall, and the final location in the laser beam. The initial polar angle is a random number from 0 to 2π, the position of the wall collision is described by polar coordinate (R,ϕ). For example, the bouncing angle ε can be generated using $\varepsilon = \arccos(-1+2\times\mathrm{rand}(1))$, where rand(1) is a random number between 0 and 1. The ending point of a trajectory is a random point within the beam.

4. Experimental and numerical results

We first compare the basic results of our model and experiments without the presence of the magnetic field gradient. Figure 4 shows a measured EIT spectrum, and figure 5 shows the calculated EIT spectra, both clearly exhibiting the expected dual structure. The broad structure linewidth is 0.2 MHz, close to the estimated transit broadening from the beam size. The narrow structure linewidth is determined by the coating, the residual magnetic field gradient within the shields, and the power broadening. Although producing qualitatively correct results, our model shows a larger linewidth than the measured one, mainly because it has not strictly taken into account of the Doppler broadening and the 3D effects as discussed below. We also compare the theoretical and the experimental narrow structure linewidths vs. the laser power at various laser beam diameters (Fig. 6), and find a good agreement in the trend. This trend is also consistent with the previously published results.[5]

Then, we studied the EIT narrow structure linewidth behavior in the presence of a magnetic field gradient. Figure 7 shows the experimental results, and figure 8 shows the theoretical results. Several trends can be identified in both the experimental and the theoretical results, which are the key results of this paper. Firstly, the linewidth increases with the increasing magnetic field gradient in a nonlinear way, i.e., the linewidth increase is slower at smaller magnetic field gradients and faster at higher

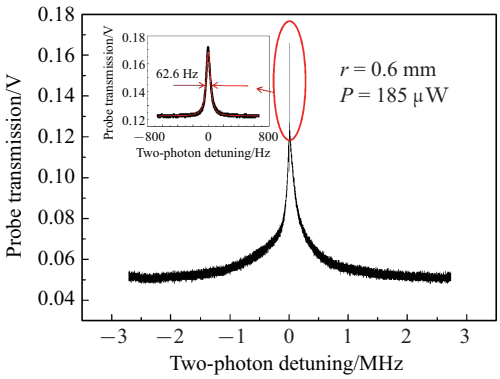


Fig. 4. (color online) Example of the measured EIT spectrum exhibiting a dual structure. The inset shows the enlarged spectrum.

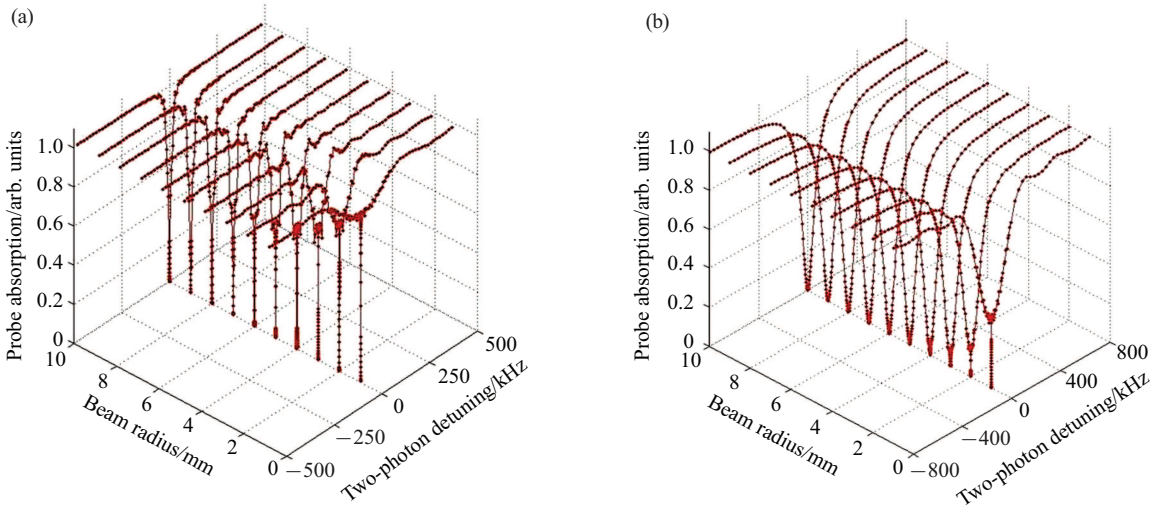


Fig. 5. (color online) Calculated EIT full lineshapes from our Monte–Carlo simulation for various beam sizes at Rabi frequencies of (a) 3 MHz and (b) 8 MHz. The narrow structure contrast decreases with increasing beam size and laser intensity due to less time outside the beam and more serious power broadening, respectively.

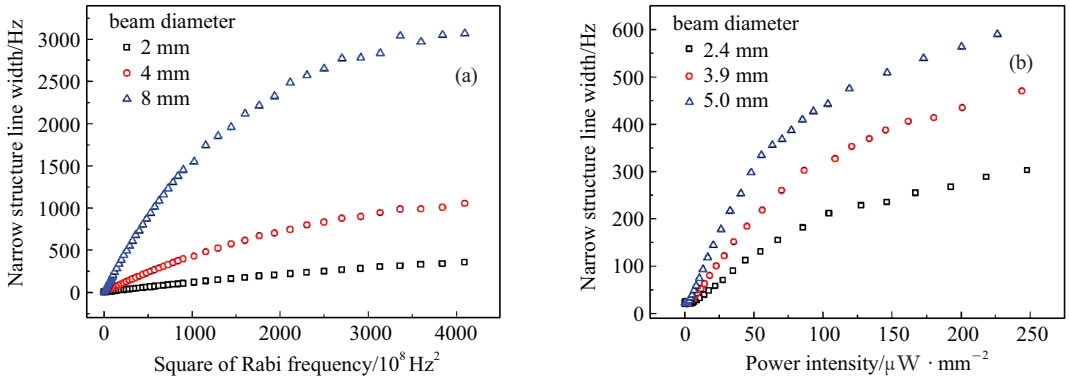


Fig. 6. (color online) Comparison of (a) theoretical and (b) experimental EIT narrow structure linewidths vs. laser power for different beam sizes, which shows the same trend that the linewidth increases with increasing laser intensity and beam size.

magnetic field gradients. Secondly, such a nonlinearity is more pronounced for the higher laser power and a larger beam size. Thirdly, for a very large laser beam size and a high laser intensity, the linewidth even shows an initial decrease with the increasing magnetic field gradient. Although the experimental and the theoretical results do not have an exact quantitative agreement, for example, in the experiment, the decrease of the linewidth with the increasing magnetic field gradient starts to happen at a smaller laser beam size and the percentage change in the linewidth is higher than that in the theory, the qualitative trends are similar.

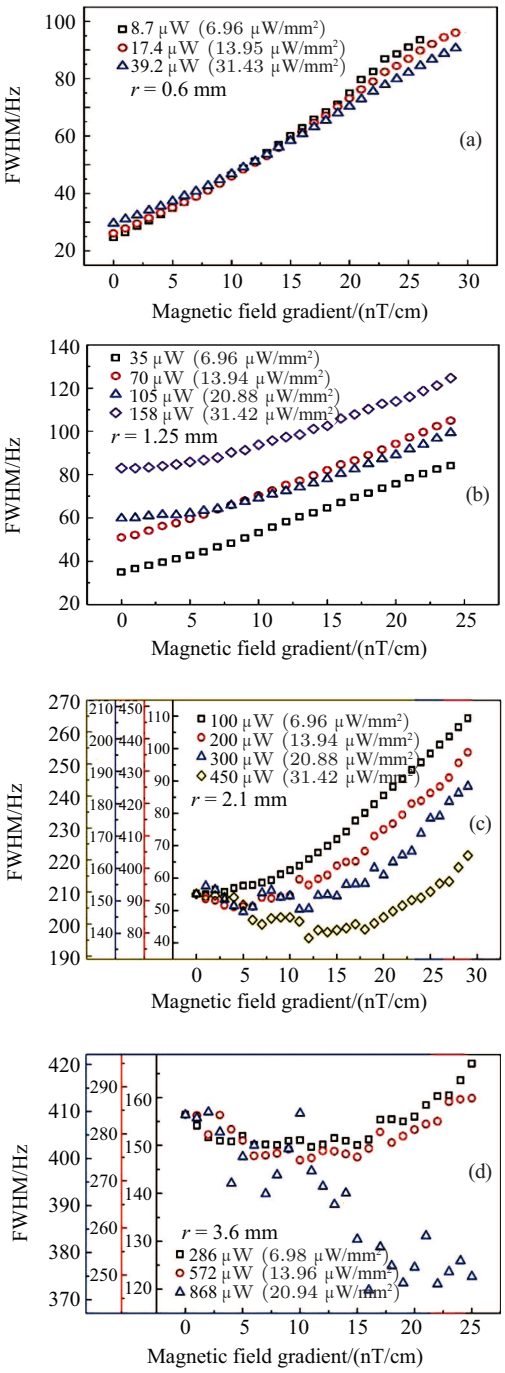


Fig. 7. (color online) Experimental results on EIT narrow structure linewidth vs. the magnetic field gradient for various laser intensities and beam sizes. In panels (c) and (d), different laser power corresponds to a different *y* axis.

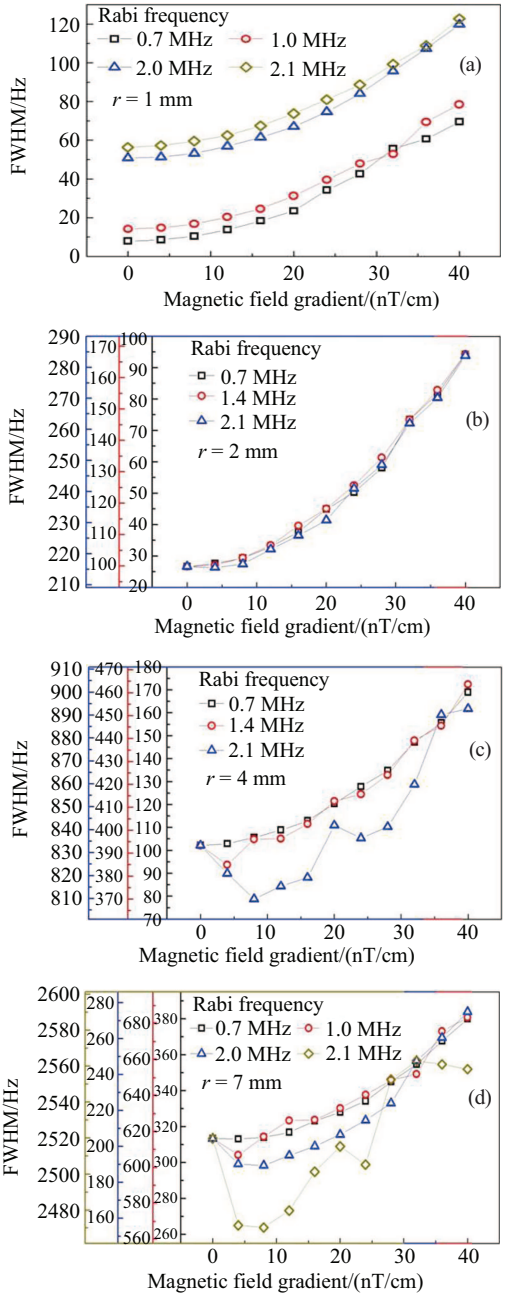


Fig. 8. (color online) Theoretical results on EIT narrow structure linewidth vs. the magnetic field gradient for various laser intensities and beam sizes. In panels (b)–(d), different laser power corresponds to a different *y* axis.

The physical explanation for the above trends is as follows. Since the narrow structure of the EIT is mainly determined by the atomic motion outside the laser beam[5] and the magnetic field variation is larger in the outside than that in the inside (because the field gradient is proportional to x), more motion outside will further broaden the width. That is why for a larger beam, the motion outside becomes less, and the percentage width broadening is smaller for small and medium magnetic field gradients. Similarly, at a higher laser power, the atoms are better optically pumped inside the beam, thus the motion outside becomes less important, and the phase accumulation outside is better washed out, that is why the percent-

age increase of the magnetic field gradient is less at a higher laser power.

The initial decrease of the EIT width is related to the linear magnetic field gradient. When the two-photon detuning is nonzero, the presence of a small field gradient makes a part of atoms inside (but towards the edge of) the laser beam on two-photon resonance. This effectively narrows the EIT narrow structure. More specifically, as our numerical calculation shows, this part of the atoms are off center from the laser beam (assuming the laser beam is centered in the cell) and spend a little more time outside between successive interactions with the laser beam, hence making the linewidth slightly smaller. From this analysis, the narrowing caused by the magnetic field gradient should be a small effect, and indeed, this decrease is only about 10% of the linewidth at most in experiments for the $D = 7.2$ mm laser beam at the highest intensity. When the magnetic field gradient becomes large enough that all atoms in the laser beam are outside the EIT resonance (the Zeeman shift in the beam is larger than the width of the EIT), the EIT linewidth starts to be larger than the zero gradient linewidth, i.e., the benefit of the magnetic field gradient on the EIT width disappears and the broadening caused by the magnetic field takes over. This argument is well supported by our experiment data summarized in Table 1. In short, an intuitive way to understand when the broadening starts is that, when the field gradient causes the Zeeman shift variation within the beam larger than the EIT full linewidth, the EIT starts to broaden.

It should be noted that our results in the low laser power and small laser beam limit are similar to those in Ref. [9], where the study was carried out for a low laser power and a small beam size. There, a quadratic dependence of the linewidth of the nonlinear magneto-optical rotation (NMOR) resonance on the magnetic field gradient was found, which was in agreement with a naive model they provided. Adapting the spirit of that model, we may also write down the EIT linewidth $\gamma_{\rm EIT}$ in the form of $\sqrt{\gamma_{\rm grad}^2 + \gamma_{\rm EIT0}^2}$, where $\gamma_{\rm grad}$ describes the broadening caused by the added field gradient, and $\gamma_{\rm EIT0}$ is the width without the field gradient. This model then leads to the following argument. At higher laser intensities and larger beam sizes, the EIT linewidth is larger, and $\gamma_{\rm EIT0}$ dominates over $\gamma_{\rm grad}$, then we have $\gamma_{\rm EIT} \approx \gamma_{\rm EIT0} + \gamma_{\rm grad}^2/(2\gamma_{\rm EIT0})$, which indicates that the broadening due to the field gradient is reduced if $\gamma_{\rm EIT0}$ is larger. This is largely consistent with our experimental results, except for the linewidth decrease at a small B gradient.

The uncertainties in the EIT linewidth data from both theory and experiments are analyzed. In the experiment, we use a polarization maintaining single mode fiber to filter the spatial mode of the laser, and the fiber has residual polarization fluctuation which is converted to intensity fluctuation by downstream polarization optics. This fluctuation is about 3%, which causes about the same level of fluctuation in the measured linewidth, as shown in Fig. 7. This also explains why the absolute amount of linewidth variation is higher for a higher total power, i.e., for higher laser intensities and larger laser beam sizes. The theoretical data display a similar situation. This is because for higher laser power, the atomic dynamics are faster, which then requires smaller time steps in the integration. The actual time step is not small enough (compromised by the computational speed), so the uncertainties in the numerical data at higher laser intensities and larger beam sizes are larger. Moreover, due to our limited computation hardware, we have only averaged over about 5000 atom trajectories, which is far less than the actual number of atoms in the experiment (approximately 10^{10} atoms per cubic centimeter).

In addition to the above sources of uncertainties, several factors contribute to the discrepancy at the quantitative level between the experimental and the theoretical results. Firstly, the atomic motion in our model is two-dimensional, while in practice the vapor cell is not infinitely long and the atomic motion in the cell is three-dimensional. Secondly, due to the computational limitation, we have not treated the Doppler broadening by integrating over all velocities, and have instead phenomenologically taken it into account by setting the excited state decay rate to 500 MHz. We find that taking into account these two factors almost closes the gap between the theoretical and the experimental linewidth values. However, since the study in this paper requires the EIT spectral calculation in a large parameter space, implementing these two corrections is

Table 1. Zeeman shift variation in the laser beam. Here, we have used 1.4 MHz/G to calculate the broadening in our model, since 0.7 MHz/G is the Zeeman splittings between adjacent magnetic sublevels, and experimentally the magnetic levels $m_{\rm f} = 2$ and $m_{\rm f} = 0$ form the EIT ground states.

Data condition (r/mm, P/mW)	Gradient at minimal EIT width (error)/nT·cm^{-1}	Corresponding Zeeman shift across laser beam (error)/Hz	Half width of EIT/Hz
2.1, 0.2	6 (1)	35.28 (5.88)	46.02
2.1, 0.3	12 (1)	70.56 (5.88)	76.08
2.1, 0.4	17 (1)	99.96 (5.88)	104.58
3.6, 0.286	7 (1)	70.56 (10.08)	78.21
3.6, 0.572	13 (2)	131.04 (10.08)	141.66

not practical due to limitations of our computational hardware. There are some other factors that also cause differences between the theoretical and experimental results. For instance, the ^{87}Rb D1 line has 16 energy levels, while the model has considered only three. In the experiment, the quantization axis may change when the two-photon detuning is close to zero and the magnetic field gradient is on, and this would switch the ground states coupled to the probe and the control fields, effectively reducing the optical pumping efficiency. However, in our model, this effect is not included. This may also explains why the linewidth decrease at a small magnetic field gradient is more obvious in the experiment than that in the numerical results.

Finally, it is worth pointing out that a similar trend was observed in a buffer gas cell previously under the situation of diffusion induced Ramsey narrowing.[8] In Ref. [8], the linewidth of the peaky part of the EIT (from a similar origin with the narrow structure of the EIT in a coated cell) was studied in buffer gas cells. The increase of the narrow structure linewidth upon a similar magnetic field gradient was found to be much slower for a higher buffer pressure than that for a lower pressure. This is because the atoms spend less time outside the laser beam in a higher buffer gas pressure, and the region outside the laser beam has a larger magnetic field variance than the region inside (due to the nature of the added linear gradient), thus the motion outside sees the broadening first. However, the decrease of the width with the added gradient was not seen in a buffer gas cell, probably because the atoms spend much less time outside the beam than in a coated cell.

5. Conclusion

In conclusion, we have theoretically and experimentally investigated the EIT linewidth behavior in a coated vapor cell in the presence of a magnetic field gradient. The nonlinear dependence of the EIT linewidth on the magnetic field gradient was found, and a novel phenomenon that the EIT linewidth decreases with the increasing magnetic field gradient in certain regimes was also identified. We obtained a good qualitative agreement between the theoretical and experimental results, and provided physical explanations for all results. This study provides a new insight to how the EIT linewidth in a coated cell broadens in the presence of a magnetic field gradient. This work is useful for EIT-based applications using a coated cell, such as quantum memory, atomic clocks, and magnetometers.

Acknowledgements

We thank Michael Hohensee for stimulating discussion, M. Balabas and D. Budker for providing the coated cell, Chen Wei-Yue for constructing the saddle coil, and Xu Xi-Wei for assistance on Labview.

References

[1] Fleischhauer M, Imamoglu A and Marangos J P 2005 *Rev. Mod. Phys.* **77** 633
[2] Balabas M V, Jensen K, Wasilewski W, Krauter H, Madsen L S, Muller J H, Fernholz T and Polzik E S 2010 *Opt. Expr.* **18** 5825
[3] Balabas M V, Karaulanov T, Ledbetter M P and Budker D 2010 *Phys. Rev. Lett.* **105** 070801
[4] Klein M, Novikova I, Phillips D F and Walsworth R L 2006 *J. Mod. Opt.* **53** 2583
[5] Klein M, Hohensee M, Phillips D F and Walsworth R L 2011 *Phys. Rev. A* **83** 013826
[6] Xiao Y H, Klein M, Hohensee M, Jiang L, Phillips D F, Lukin M D and Walsworth R L 2008 *Phys. Rev. Lett.* **101** 043601
[7] Watanabe S F and Robinson H G 1977 *J. Phys. B: Atom. Molec. Phys.* **10** pp. 931–939, 941–957, 959–965
[8] Novikova I, Xiao Y H, Phillips D F and Walsworth R L 2005 *J. Mod. Opt.* **52** 2381
[9] Pustelny S, Jackson Kimball D F, Rochester S M, Yashchuk V V and Budker D 2006 *Phys. Rev. A* **74** 063406
[10] Xiao Y H, Novikova I, Phillips D F and Walsworth R L 2006 *Phys. Rev. Lett.* **96** 043601
[11] Xiao Y H, Novikova I, Phillips D F and Walsworth R L 2008 *Opt. Expr.* **16** 14128
[12] Ramsey N F 1956 *Molecular Beams* (Oxford: Clarendon)
[13] Shahriar M S, Hemmer P R, Katz D P, Lee A and Prentiss M G 1997 *Phys. Rev. A* **55** 2272
[14] Budker D, Hollberg L, Kimball D F, Kitching J, Pustelny S and Yashchuk V V 2005 *Phys. Rev. A* **71** 012903
[15] Steckelmacher W 1986 *Rep. Prog. Phys.* **49** 1083
[16] Feres R and Yablonsky G 2004 *Chemical Engineering Science* **59** 1541